

Spatial distribution of thermal properties on debris-covered glaciers in the Himalayas derived from ASTER data

Ryohei SUZUKI, Koji FUJITA and Yutaka AGETA

Graduate School of Environmental Studies, Nagoya University, Nagoya 464-8601, Japan

(Received August 31, 2006; Revised manuscript accepted November 13, 2006)

Abstract

The present study investigates thermal resistances on debris-covered glaciers around Mt. Everest and in the Lunana region of Bhutan, using satellite images taken by ASTER and NCEP/NCAR reanalysis data. The thermal resistance is defined as the thickness divided by the thermal conductivity of a debris layer, and is an important index to the evolution of glacial lakes through the melting process. This index is obtained from surface temperature and heat balance on the debris layers. Since the net radiation is a dominant energy source on the Himalayan glaciers, thermal resistances are calculated by neglecting turbulent heat flux in heat balance. We evaluate errors of thermal resistances using field meteorological data and multitemporal ASTER data. The result shows that above errors are unlikely to affect the spatial pattern of thermal resistances. About half of 25 target glaciers without moraine-dammed lakes have larger thermal resistances than 7 glaciers with the lakes. Spatial distribution of thermal resistances shows the large increases toward glacier termini on the glaciers without lakes, whereas relatively small and uniform values on those with lakes. These results imply that the difference in magnitudes and distribution of thermal resistances on debris-covered glaciers are related to different evolutionary stages of the glacial lakes in the Himalayas. The present study demonstrates the possibility that ASTER data provide thermal resistance distribution over many glaciers for glacial lake studies without simultaneous field observations.

1. Introduction

Many studies have reported that debris-covered glaciers generate moraine-dammed glacial lakes (Yamada, 1998; Ageta *et al.*, 2000; Richardson and Reynolds, 2000; Komori *et al.*, 2004). The potential hazards of Glacial Lake Outburst Flood (GLOF) in the Himalayas are attributed to the rapid retreat of glaciers in this region (*e.g.*, Yamada, 1998; Ageta *et al.*, 2000; Komori *et al.*, 2004; Quincey *et al.*, 2005). However, physical processes controlling expansion of the moraine-dammed glacial lakes are still uncertain. Revealing what determines the presence of glacial lakes is particularly crucial and practical for hazard assessment. Thus, investigation of the differences between debris-covered glaciers with lakes and those without lakes is needed.

Reynolds (2000) suggested that a glacier's surface gradient is a controlling factor in the formation of supraglacial ponds. He mentioned that ice melting is also an essential controlling factor because it interacts with the glacier's surface gradient and is a source of meltwater itself. Regardless of such a direct link, the

extensive spatial characteristics of glacier melting under debris layer have never been studied in relation to the presence of glacial lakes in the Himalayas.

Here we focus on thermal properties of supraglacial debris as another possible controlling factor in different evolutionary stages of glacial lakes in the Himalayas, as ice melting depends on the thermal properties (*e.g.*, Fujii, 1977; Lundstrom *et al.*, 1993; Mattson *et al.*, 1993; Diolaiuti *et al.*, 2003). However, the thermal properties such as thickness and thermal conductivity of debris layers are so heterogeneous even on a glacier that field observation is not practical. Satellite remote sensing is an effective technique for mapping surface characteristics regarding glacier melting. Rana *et al.* (1997) and Nakawo and Rana (1999) demonstrated a method to estimate the melt rate of a debris-covered glacier in the Nepal Himalayas using Landsat TM images. They applied the idea of thermal resistance which was defined by Nakawo and Young (1981; 1982) as thickness divided by thermal conductivity of a debris layer. The thermal resistance at a specific site can be regarded as constant usually in a melting season. Rana *et al.* (1997) proposed this parameter for runoff modeling and showed

that the modeled runoff was in good agreement with the observed value. The advantage of this methodology is that heterogeneous thermal resistances on a debris-covered area can be smoothed by moderate resolution of satellite images as a mixed pixel value (Nakawo *et al.*, 1993). Supraglacial ponds which are distributed on debris-covered areas play a significant role in evolution of glacier lakes (*e.g.*, Sakai *et al.*, 2000). Mapping their distributions and estimating their contribution to ice melting is not easy without remote sensing techniques. Utilization of satellite images providing moderate resolution and multispectral bands, such as Advanced Spaceborne Thermal Emission and Reflection Radiometer (ASTER), has proved to be quite valuable in glaciology (*e.g.*, Wessels *et al.*, 2002; Kargel *et al.*, 2005; Quincey *et al.*, 2005). The aim of the present paper is to show that extensive distribution of thermal resistances can be obtained from ASTER data independently from ground observations. Relationship between thermal resistances on debris-covered glaciers and the presence of moraine-dammed glacial lakes with an area larger than that corresponding to a pixel size (approximately 0.01 km²) around the Mt. Everest region of Nepal and China are shown to demonstrate that ASTER data are useful for study on processes of glacial lake formation. Thus, spatial comparison of the thermal resistances distributed on multiple glaciers over this extensive area is important for our purpose rather than absolute or high-detailed spatial resolution measurements on a limited number of glaciers.

2. Methods

2.1 Thermal resistance of a debris layer

The thermal resistance of a debris layer has been utilized as a useful index for ice melting of individual glacier so far. Thermal resistance is defined as

$$R = \frac{h}{\lambda}, \quad (1)$$

where R , h and λ are thermal resistance (m²K W⁻¹), the thickness (m) and thermal conductivity (m⁻¹K⁻¹W) of a debris layer, respectively (Nakawo and Young, 1981; 1982). Because conductive heat into glacier ice is negligible on temperate glaciers, a thermal resistance can be derived from the following equation based on the assumptions that the temperature profile within a debris layer is linear and bottom temperature is 0°C due to ice melting:

$$C = \frac{T_s - 0}{R}, \quad (2)$$

where C is heat conducted into a debris layer (W m⁻²) and used for ice melting, and T_s is surface temperature of the debris layer (°C). The C is calculated by the heat balance equation

$$C = R_n + H + E, \quad (3)$$

where R_n , H and E are fluxes for net radiation, and sensible and latent heats, respectively. The unit of all variables is W m⁻². All components are positive when fluxes are directed towards the debris surface. Turbulent heat flux, which is composed of H and E , can be usually estimated using the bulk aerodynamic method (*e.g.*, Rana *et al.*, 1997; Kayastha *et al.*, 2000). Mattson and Gardner (1991) observed energy exchange on a debris-covered glacier in Karakoram and found a negligible contribution of the turbulent heat fluxes to the total energy exchange on a clear sky day in melting season. The same characteristic that radiation is a main energy exchange source is also reported in the Himalayas by Ohata and Higuchi (1980), Kayastha *et al.* (2000), Takeuchi *et al.* (2000), among others. For the present analysis it is shown that turbulent heat fluxes on glaciers do not significantly affect the relationship between heat balance and thermal resistances from analyses using data in the Lunana region of Bhutan. Based on the analyses, spatial distribution of thermal resistances around Mt. Everest is calculated by neglecting turbulent heat fluxes. Uncertainties in thermal resistances due to neglecting turbulent heat fluxes are discussed in section 3.1.

2.2 Meteorological data

The relation between heat balance components and thermal resistances was investigated using field meteorological data which correspond to ASTER data acquisition. Such data sets are available only in the Lunana region of Bhutan (Fig. 1). Hence, the ground meteorological data which were obtained from an automatic weather station (AWS) at 4524 m a.s.l. on the terminal dead ice zone of Lugge Glacier (Yamada *et al.*, 2004; Suzuki *et al.*, 2007) were used in our analysis. Table 1 shows the mean meteorological compo-

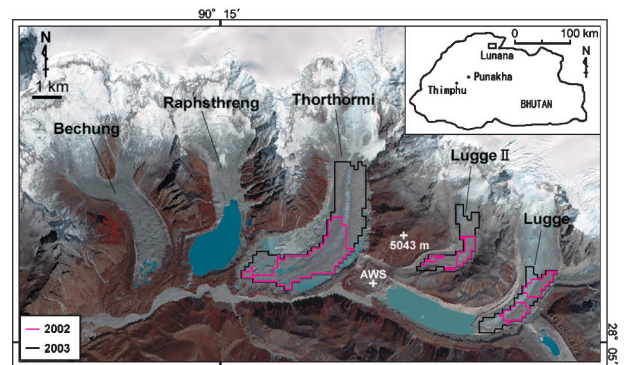


Fig. 1. False color composite image of Lunana region, Bhutan taken by ASTER VNIR band 1, 2, 3N on 21 November 2001. Names of objective glaciers are also shown. Two crosses denote locations of stations with AWS and air temperature sensor. Violet and black solid lines denote entire target areas in 2002 and 2003, respectively.

Table 1. Input meteorological data to calculate thermal resistances on three glaciers in Lunana region of Bhutan. Data were obtained from AWS installed at 4524m a.s.l. on terminal moraine-covered ice zone of Lugge Glacier. All data shown are mean values from 10:30 to 11:00 in local time, during which ASTER data were acquired. Ws: wind speed; Wd: wind direction; Ta: air temperature; rh: relative humidity; SD: downward shortwave radiation; SU: upward shortwave radiation; Rn: net radiation; Ts: surface temperature.

Date	Ws m s ⁻¹	Wd deg.	Ta °C	rh %	SD W m ⁻²	SU W m ⁻²	Rn W m ⁻²	Ts °C
20 September 2002	1.7	292.6	8.1	40.3	938	186	633.8	20.4
21 July 2003	2.7	327.6	12.2	45.9	1074	187	652.4	27.9

Table 2. ASTER data description.

Year	Date	Path/Row	Target	Level	Usage
2000	28 September	140/116	Nepal	1B	VNIR, TIR
2000	14 October	140/116	Nepal	1B	VNIR, TIR
2001	27 June	140/116	Nepal	1B	VNIR, TIR
2002	20 September	138/115	Bhutan	1B	VNIR, TIR
2002	4 October	140/116	Nepal	1B	VNIR, TIR
2002	21 November	140/116	Nepal	3A01	DEM
2003	1 June	140/116	Nepal	1B	VNIR, TIR
2003	21 July	138/115	Bhutan	3A01	VNIR, SWIR, TIR
2003	23 October	140/116	Nepal	1B	VNIR, TIR
2004	9 October	140/116	Nepal	1B	VNIR, TIR
2004	10 November	140/116	Nepal	3A01	DEM

nents at every 30 minutes for two ASTER data acquisitions in 2002 and 2003. The meteorological data are extrapolated to the whole target areas to solve the heat balance equation for the thermal resistances. The observed air temperatures were corrected for each altitude using an averaged lapse rate of 6.1°C km⁻¹ obtained from field observations which were carried out from 29 September to 8 October in 2003 (Suzuki *et al.*, 2007). On the other hand, products of surface downward radiation fluxes for clear sky at 0600Z from National Centers for Environmental Prediction (NCEP)/National Center for Atmospheric Research (NCAR) reanalysis (Kalnay *et al.*, 1996), which corresponds to the nearest time and location to each ASTER data acquisition, were used to calculate thermal resistances on glaciers around Mt. Everest.

2.3 ASTER data

ASTER data are composed of visible and near infrared (VNIR), shortwave infrared (SWIR) and thermal infrared (TIR) bands. Table 2 provides a description of ASTER data that were used for the present calculations. Because of the assumption that the bottom temperature of a debris layer equals 0°C (Eq. 2), we chose the data taken in glacier melt seasons except for producing the digital elevation model (DEM). In addition, data with cloud or snow cover on debris-covered areas were not used. Due to these con-

strained conditions, the number of available images was limited to 11 (Table 2).

All images were rectified based on the orthorectified product Level 3A01 of ASTER and resampled by the nearest-neighbor method. Only the glacierized areas above 0°C were extracted from each data because debris surfaces are warmed on a clear sky morning. Altitudes at the extracted pixels were obtained from DEM which were appended to the Level 3 A01 product. The DEM data, which are generated using the instrument and the spacecraft ephemeris parameters only without referring to ground control points for individual images, is produced by the ASTER Ground Data System (ASTER GDS) at the Earth Remote Sensing Data Analysis Center (ERSDAC) in Japan using specially developed DEM software (Fujisada *et al.*, 2005).

Average brightness temperature was calculated from five TIR bands at each acquisition time and used as surface temperature on glaciers. Spectral reflectance at the top of atmosphere in VNIR bands was averaged to estimate broadband albedo. Downward spectral irradiances were varied according to solar angles at each ASTER acquisition time and location. Pixel size of all images was unified to 90 m of TIR bands, and thermal resistances were calculated using the same resolution.

Band 4 (1.6–1.7 μm) in SWIR was combined with

band 2 (0.63–0.69 μm) in VNIR to calculate the Normalized Difference Water Index (NDWI) on glaciers in the Lunana region of Bhutan. This index can show the presence of water surface based on a spectral characteristic of water that corresponds to stronger absorption in the wavelength of SWIR bands than those in VNIR bands (McFeeters, 1996). NDWI is defined as

$$NDWI = \frac{Band2 - Band4}{Band2 + Band4}, \quad (4)$$

where positive NDWI indicates the presence of open water surface including melting surface of snow, ice and debris saturated with water.

3. Results and discussion

3.1 Uncertainties in thermal resistances

In this section, uncertainties in thermal resistances due to neglecting turbulent heat fluxes (section 2.1) and total errors are identified and discussed. In order to address the issue, three debris-covered glaciers in the Lunana region of Bhutan (Fig. 1) were the focus. The areas covered with cloud on the target glaciers in 2002 were extracted manually and eliminated from calculation.

Figure 2 shows two type calculations of thermal resistances; one is calculated from all components in heat balance equation (Eq. 3) and the other is approximated from only net radiation term. The former is obtained in two ways under water saturated and dry surface assumptions. Sensible heat term is not important because thermal resistances based on dry surface assumptions nearly equal those from only net radiation. In contrast, large differences are found in

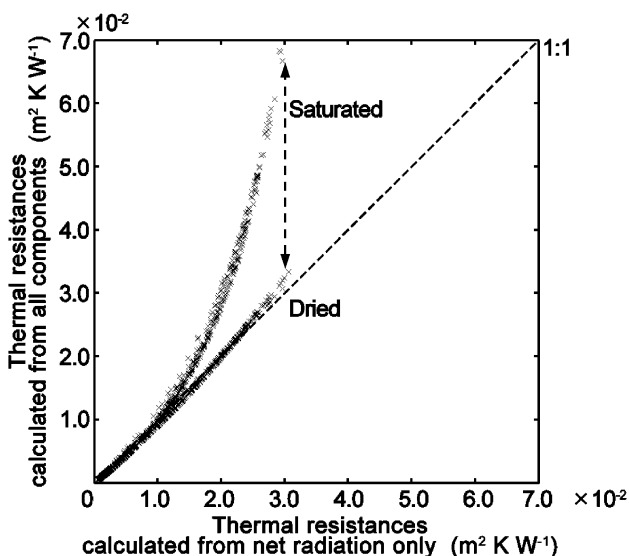


Fig. 2. Relations between thermal resistances calculated from only net radiation and from all components of the heat balance equation at same pixel. Two curves indicate ultimate values depending on moisture difference on debris layers.

wet condition between approximation and analytic solutions. Since surface temperature of a debris layer increases in association with larger thermal resistances, saturated vapor pressure on the debris layer also increases under the water-saturated condition. Thus, such large differences in thermal resistances can be caused by the increase of latent heat flux.

As the presence of water affects the magnitude of a thermal resistance, water saturated areas were estimated using NDWI, which was calculated from band 2 and band 4 of ASTER data. Figure 3a shows transverse profiles of NDWI and surface temperatures that were obtained from ASTER images of Thorthormi Glacier in Lunana region. The moisture dominant ranges such as central ogive and lateral ponds (Fig. 3 b, Fig. 3c), where low surface temperatures near 0°C appear, are identified by positive NDWI, while NDWI in debris-covered areas and lateral moraines, where high temperature appears, are negative values. Figure 4 shows the relationship between NDWI and thermal resistances on three debris-covered glaciers in Lunana region (Fig. 1). Thermal resistances in the positive NDWI range are found to be less than $2.0 \times 10^{-2} \text{ m}^2 \text{ K W}^{-1}$, which produces negligible differences between dry and wet surface assumptions (Fig. 2). This is because the low temperature surroundings of melting ice generate only small differences in vapor pressures between atmosphere and debris. On the other hand, a thick debris-covered area is generally dry on a clear sky morning in the Himalayas (Mattson and Gardner, 1991). It is plausible assumption that the water-saturated case in Fig. 2 hardly occurred in the debris-covered area on a clear day of ASTER data acquisition. As mentioned above, neglected turbulent heat fluxes do not contribute significantly to the thermal resistance calculation.

On the other hand, total errors are also evaluated by comparing independent observations in 2002 and 2003 (Tables 1 and 2) of the three glaciers. Figure 5 shows a comparison of thermal resistances calculated from only net radiation. Note that the thermal resistance at a specific pixel may be affected by the ice movement and deposition of supraglacial debris between two ASTER data acquisitions, because surface flow speeds on the analyzed area of Thorthormi Glacier range from 40 to 100 m a^{-1} (Yamada *et al.*, 2004; Kääh, 2005), while the pixel size is 90 m square. Hence, the error shown in Fig. 5 is composed of systematic error due to ice movement as well as random error propagated through each measurement.

Thermal resistance in 73% of the terminal area of the Ngozumba Glacier in Nepal (see the next section) was calculated from 7 independent ASTER data (Table 2) and corresponding NCEP/NCAR reanalysis data. The residual area was not available for the calculation due to cloud cover. The averaged thermal resistance equals $3.1 \times 10^{-2} \text{ m}^2 \text{ K W}^{-1}$, while the

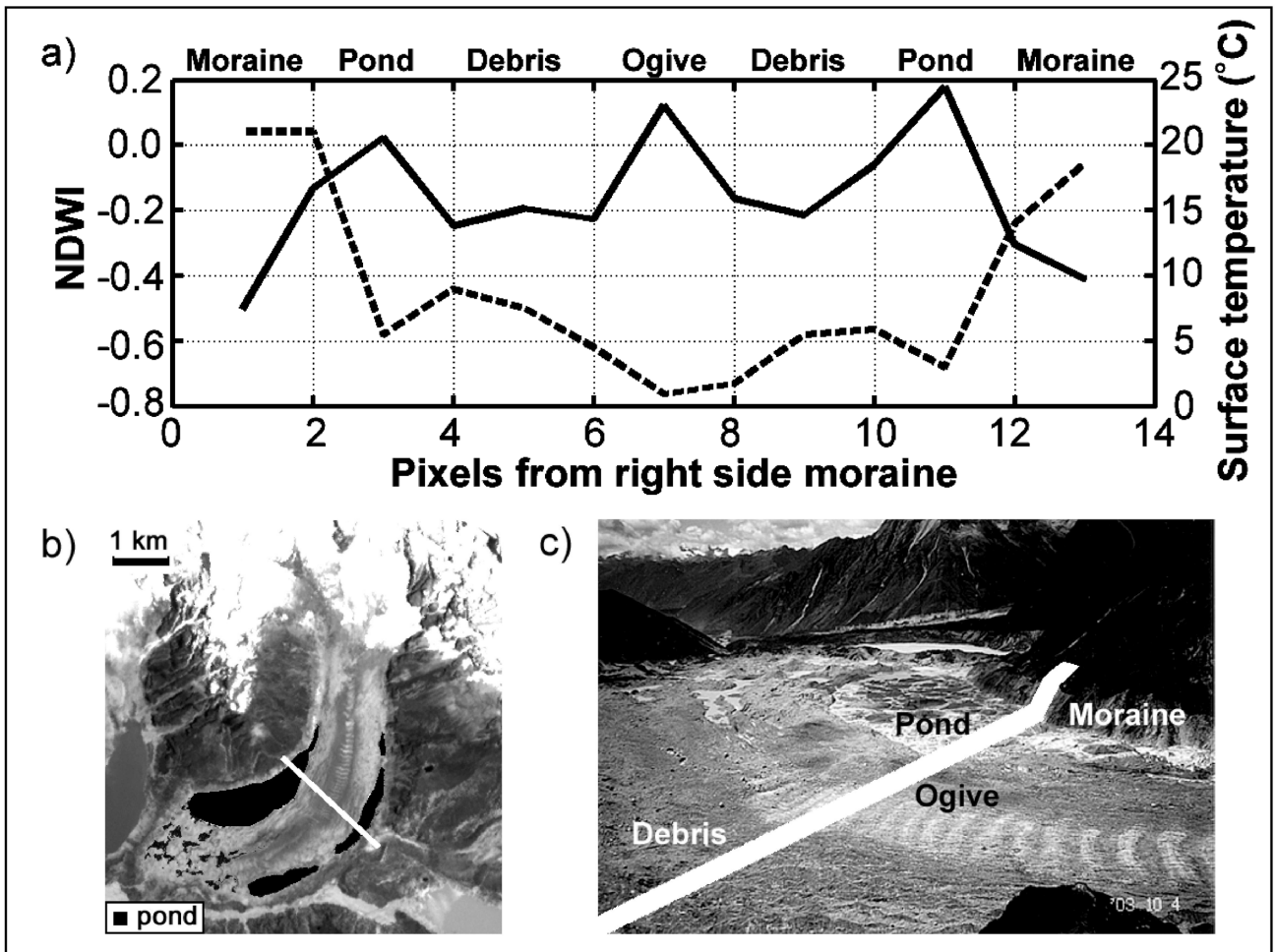


Fig. 3. a) Transverse profiles of NDWI (solid line) and surface temperature (broken line) obtained from ASTER data on Thorthormi Glacier in Lunana region of Bhutan. b) Image taken by ASTER-VNIR. White solid line indicates location of transverse profile shown in a). c) Corresponding photograph shows glacier surface. Upper right in photo shows right-bank side moraine, and lower left reveals thickly debris-covered area. Thick white line drawn indicates location of transverse profile.

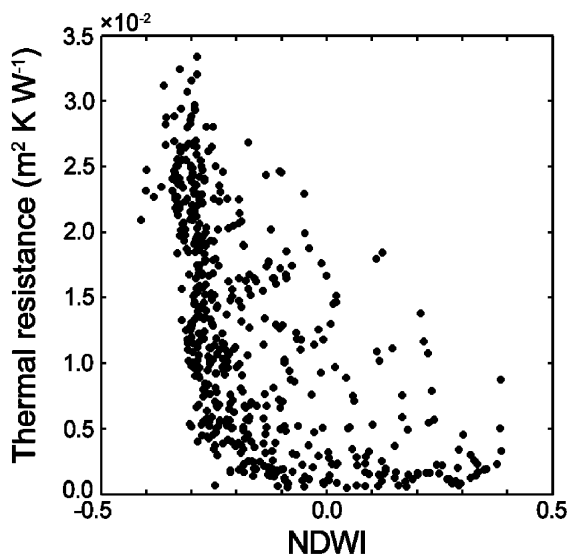


Fig. 4. Relation between NDWI and thermal resistances on three debris-covered glaciers in Lunana region of Bhutan.

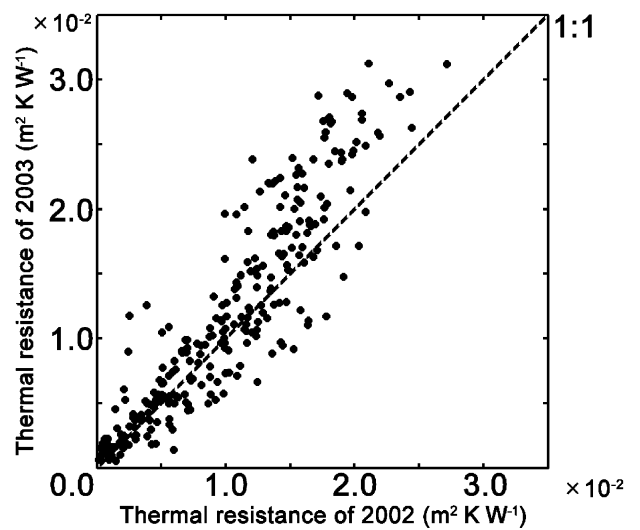


Fig. 5. Relation between thermal resistances in 2002 and those in 2003 at same pixels for three debris-covered glaciers in Lunana region of Bhutan.

standard deviation equals $0.35 \times 10^{-2} \text{ m}^2 \text{ K W}^{-1}$. This result means that thermal resistances from independent data are not biased significantly, because the deviations are less than those shown in Fig. 5 despite the abovementioned change in surface condition. Because available data can be obtained from ASTER only on a clear sky morning, the reanalysis data under clear sky conditions were chosen as input radiation fluxes. Additionally, the density of air is relatively thin due to the high altitude of the target areas. These conditions cause less variation in atmospheric conditions such as the amount of water vapor and small turbulent heat flux at each acquisition of ASTER data. Thus, the net radiation obtained by combining reanalysis data with ASTER data is considered to be useful for deriving thermal resistance distribution, because neglecting turbulent heat flux in the heat balance equation does not pose a serious problem for our study. In the following section, thermal resistances on multiple debris-covered glaciers are calculated using net radiation obtained from these data and neglecting turbulent heat flux.

3.2 Spatial distribution of thermal resistances

Figure 6 shows a mosaic image of thermal resistance around Mt. Everest. The western and eastern parts of the image were calculated from ASTER data taken in 28 September 2000 and 23 October 2003, respectively. In addition, thermal resistances on three

debris-covered glaciers in the Lunana region of Bhutan (Fig. 1) were derived using NCEP/NCAR reanalysis data inputs. Totally, 32 debris-covered glaciers were analyzed in this study. Figure 7 shows the frequency distribution of thermal resistances averaged for each debris-covered area. Means of two groups were obtained from the data; 7 glaciers with lakes had a mean thermal resistance of $1.6 \times 10^{-2} \text{ m}^2 \text{ K W}^{-1}$, while 25 glaciers without lakes had $2.4 \times 10^{-2} \text{ m}^2 \text{ K W}^{-1}$.

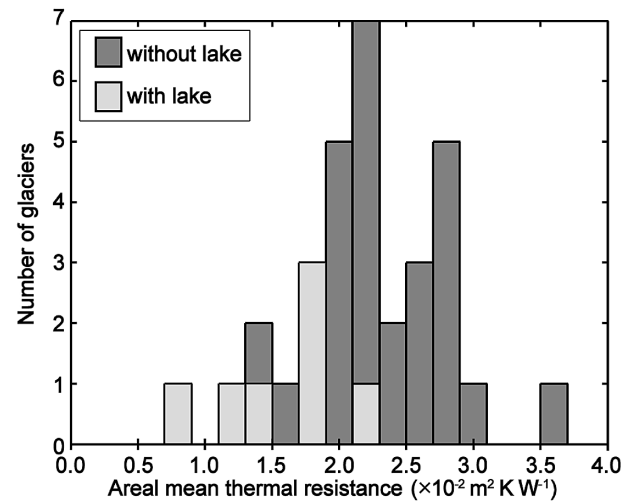


Fig. 7. Frequency distribution of areal mean thermal resistances on glaciers with and without lakes.

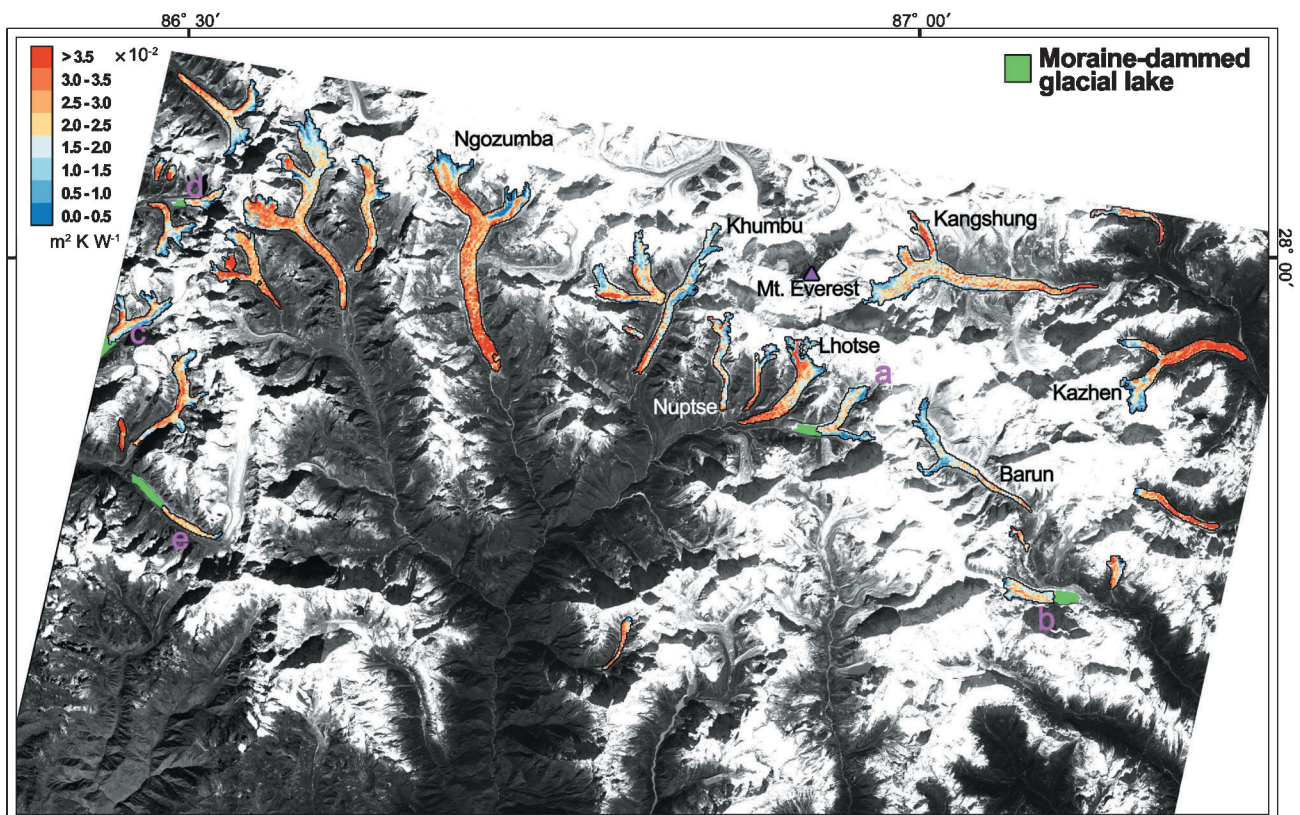


Fig. 6. Distribution of thermal resistances on debris-covered glaciers around Mt. Everest.

The errors discussed in the previous section make it difficult to distinguish exactly the thermal resistances among all the target glaciers with and without lakes (Fig. 7). However, we found that 12 glaciers without lakes having a larger thermal resistances than the maximum of glaciers with lakes. This means that ice melting on these glaciers is more strongly controlled by the debris cover than on glaciers with lakes. The higher surface temperature will be generated in case a debris layer has higher thermal resistance. A negative energy balance through the increase of upward longwave radiation can occur under such a condition even if the climatic condition is uniform. Thus, the ice melt rate decreases with the increase in thermal resistance.

The residual 13 glaciers without lakes such as Khumbu Glacier (Fig. 6) do not show a definite difference in areal mean thermal resistances compared to those with lakes. Complex surfaces that are composed of supraglacial ponds, ice cliffs and bare ice areas as well as debris cover resulted in relatively small thermal resistances, because such various surfaces with low temperature are mixed in pixels of ASTER images. Therefore, the thermal resistance is reduced and appropriate conditions for ice melting is produced. In fact, Sakai *et al.* (2000) found that the amount of energy absorption on a supraglacial pond is more than several times that on debris-covered area and suggested that the rapid ice melting accelerates evolution of supraglacial ponds. Iwata *et al.* (2000) reported that the area with a rough uneven surface with large relative relief had extended both upglacier and downglacier recently. This fact leads to lowering of thermal resistance on the glacier, which will cause a depression in the lower ablation area as predicted by a numerical simulation (Naito *et al.*, 2000).

Figure 8 shows the relation between distributions of thermal resistance and debris thickness on the Khumbu Glacier in Nepal. Conway and Rasmussen (2000) reported a thermal conductivity of $1.28 \text{ W m}^{-1} \text{ K}^{-1}$ of the debris layer 2.5 m thick on this glacier. The data resulted in a thermal resistance of $2.0 \text{ m}^2 \text{ K W}^{-1}$, about hundred times as large as shown in Fig. 8. Such low thermal resistance obtained from Landsat TM data was also reported in other studies (*e.g.*, Rana *et al.*, 1997). This discrepancy is caused because surfaces of ice cliffs and small ponds as well as debris are observed as a mixed pixel value of satellite data, whereas Conway and Rasmussen (2000) observed only debris in the field observation. Thickness of debris is in proportion to thermal resistance as described in Eq. 1. This relation can be seen in Fig. 8. The decrease of thermal resistances on the eastern side of the glacier in the area several kilometers from the terminus can be explained by the areas of expanding ponds and developing ice cliffs as reported by other studies (*e.g.*, Iwata *et al.*, 2000). If only the eastern part of this

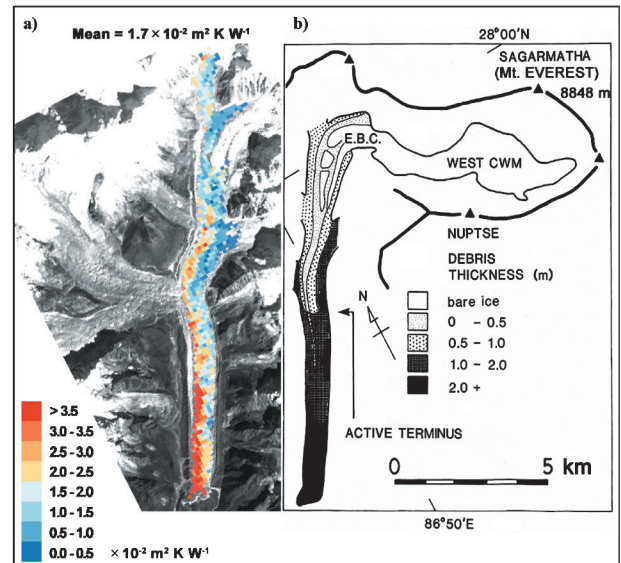


Fig. 8. Distributions of a) thermal resistances and b) debris thickness (reprinted from Nakawo *et al.*, 1986 by permission of International Glaciological Society) on Khumbu Glacier in Nepal, respectively.

glacier was shaded in the morning of ASTER data acquisition, surface temperatures in this area would be lower than those on the western part. This apparently generates a similar pattern of thermal resistances. In this case, surface temperatures outside of the glacier would also decrease from west to east. However, only negligible differences of surface temperature can be recognized outside of the glacier itself along the side moraines. Thus, shading of solar insolation by surrounding mountains may not cause the decrease of thermal resistances. Thermal resistances increase gradually along flow directions as a thickness pattern. As Fig. 6 shows, a similar pattern can be found on the other glaciers without lakes.

In order to investigate spatial characteristics of thermal resistances, relations with altitudes are shown in Figs. 9 and 10 in terms of glaciers without lakes and with lakes, respectively. The glaciers in Fig. 9 were selected based on areal mean thermal resistances which range from 1.5×10^{-2} to $2.7 \times 10^{-2} \text{ m}^2 \text{ K W}^{-1}$ as shown in Fig. 7 to represent the glaciers without lakes. Thermal resistances increase toward downstream on 22 glaciers among all the glaciers without lakes, whereas different variations that are relatively uniform magnitudes are found on glaciers with lakes. Spatial analysis of thermal resistances can be applied to assessment of glacier lake formation by combining the other spatial information, for example, ice dynamics and surface slopes, because surface lowering of glacier is related to mass balances and ice velocity gradients along flow lines. Multispectral satellite data are useful for assessment of glacial lake formation.

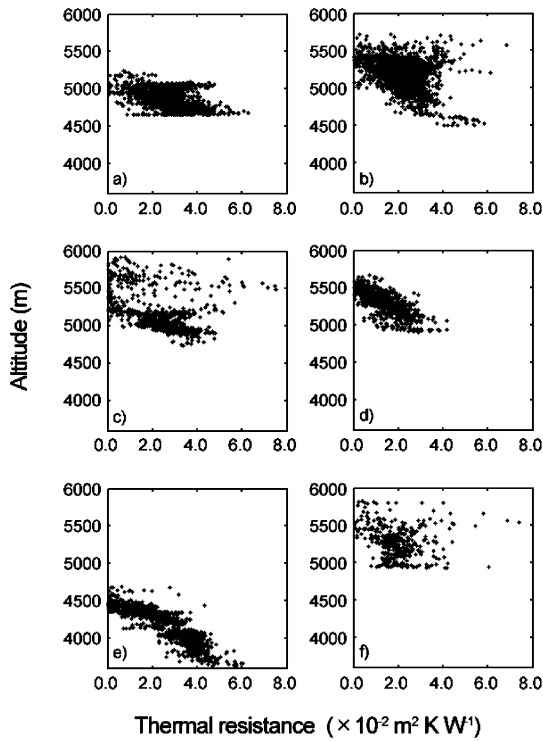


Fig. 9. Relations between thermal resistances and altitudes of glaciers without lakes; a) Ngozumba, b) Kangshung, c) Lhotse, d) Barun, e) Kazhen and f) Nuptse Glaciers in Fig. 6.

4. Conclusion

Spatial distribution of thermal resistances in the Mt. Everest region was derived applying extensive satellite remote sensing to investigate relationship between the magnitudes of thermal resistances and the presence of moraine-dammed glacial lakes. We focused on thermal resistances as a relative index of glacier melting, whereas previous works only aimed to estimate absolute melt rates for limited glaciers. Our analysis showed that the errors from neglecting turbulent heat fluxes in heat balance calculation and using multitemporal ASTER data are unlikely to affect the spatial pattern of thermal resistances. This means that, to clarify the physical processes, the spatial distribution of thermal resistances can be obtained by remote sensing techniques and related to spatial information about the surface gradient and ice velocity which have also been proved to be important conditions for glacier lake expansion (Richardson and Reynolds, 2000; Quincey *et al.* 2006). Thermal resistances on glaciers with lakes tended to be smaller than on those without lakes. Furthermore, different altitudinal and flow-line patterns of thermal resistance distribution were identified in association with the presence of glacial lakes. These results suggest

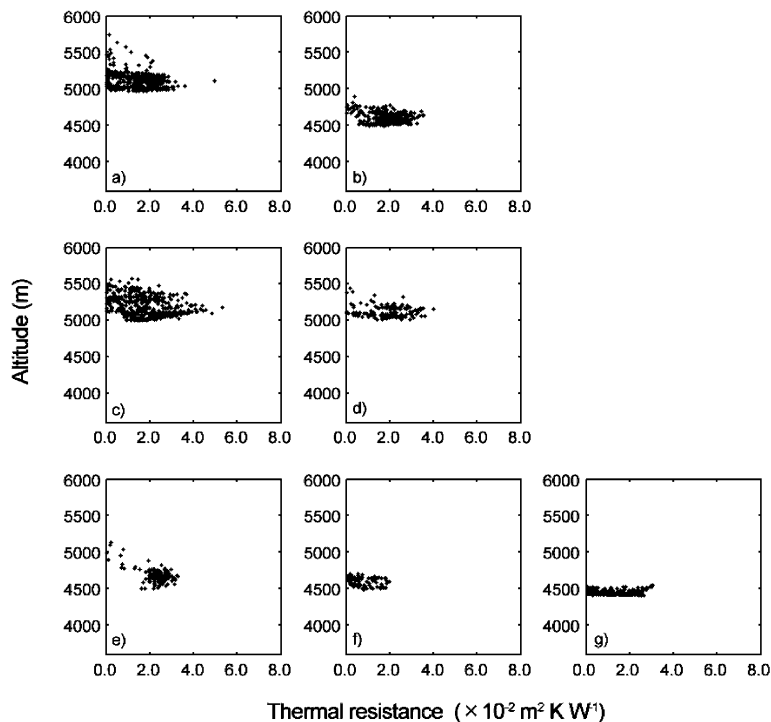


Fig. 10. Relations between thermal resistances and altitudes of glaciers with lakes. Letters in these figures correspond to those in Fig. 6: a) Lhotse Shar, b) Lower Barun, c) Drogpa Nagtsang, d) unnamed glacier on available map, and e) Trambau Glaciers. Figures f) and g) correspond to Lugge and Thorthormi Glaciers shown in Fig. 1, respectively.

that the thermal resistance of debris-covered glaciers would be a useful index to study glacial lake evolution, and that ASTER data are also useful for such analyses. The other dominant processes of glacial lake formation should also be identified to establish more general criteria for future hazard assessments.

Acknowledgments

Many people generously cooperated in obtaining data from the field observations for this study. In particular, we are grateful to the Geological Survey of Bhutan. The manuscript was much improved by useful comments from Dr. Nozomu Naito, Dr. Masayoshi Nakawo and Dr. Howard Conway. The copyright for ASTER data is reserved by the Ministry of Economy, Trade and Industry of the Japanese Government. This study was supported by the Announcement of Research Opportunity (ASTER ARO, AP-0006) and a Grant-in-Aid for Scientific Research (Project: 13373006; 13573004; G-4, the 21st Century COE Program) from the Ministry of Education, Culture, Sports, Science and Technology of Japan. Figure 8b was reprinted from the *Annals of Glaciology* with the permission of the International Glaciological Society.

References

- Ageta, Y., Iwata, S., Yabuki, H., Naito, N., Sakai, A., Narama, C. and Karma (2000): Expansion of glacier lakes in recent decades in the Bhutan Himalayas. *In* Nakawo, M., Raymond, C.F. and Fountain, A. (eds.), *Debris-Covered Glaciers*, IAHS Publ., **264**, 165–175.
- Conway, H. and Rasmussen, L.A. (2000): Summer temperature profiles within supraglacial debris on Khumbu Glacier, Nepal. *In* Nakawo, M., Raymond, C.F. and Fountain, A. (eds.), *Debris-Covered Glaciers*, IAHS Publ., **264**, 89–97.
- Diolaiuti, G., D'Agata, C. and Smiraglia, C. (2003): Belvedere Glacier, Monte Rosa, Italian Alps: tongue thickness and volume variations in the second half of the 20th century. *Arc. Antarc. Alp. Res.*, **35**, 255–263.
- Fujii, Y. (1977): Field experiment on glacier ablation under a layer of debris cover. *Seppyo*, **39**, Special issue, 20–21.
- Fujisada, H., Bailey, G.B., Kelly, G.G., Hara, S. and Abrams, M. J. (2005): ASTER DEM performance. *IEEE T. Geosci. Remote*, **43**, 2707–2714.
- Iwata, S., Aoki, T., Kadota, T., Seko, K. and Yamaguchi, S. (2000): Morphological evolution of the debris cover on Khumbu Glacier, Nepal between 1978 and 1995. *In* Nakawo, M., Raymond, C.F. and Fountain, A. (eds.), *Debris-Covered Glaciers*, IAHS Publ., **264**, 3–11.
- Kääb, A. (2005): Remote sensing of mountain glaciers and permafrost creep. *Geographisches Institut der Universität Zürich*, 266 pp.
- Kalnay, E., Kanamitsu, M., Kistler, R., Collins, W., Deaven, D., Gandin, L., Iredell, M., Saha, S., White, G., Woollen, J., Zhu, Y., Chelliah, M., Ebisuzaki, W., Higgins, W., Janowiak, J., Mo, K.C., Ropelewski, C., Wang, J., Leetmaa, A., Reynolds, R., Jenne, R. and Joseph, D. (1996): The NCEP/NCAR 40-year reanalysis project. *Bull. Am. Meteorol. Soc.*, **77**, 437–471.
- Kargel, J.S., Abrams, M.J., Bishop, M.P., Bush, A., Hamilton, G., Jiskoot, H., Kääb, A., Kieffer, H.H., Lee, E.M., Paul, F., Rau, F., Raup, B., Shroder, J.F., Soltesz, D., Stainforth, D., Stearns, L. and Wessels, R. (2005): Multispectral imaging contributions to global land ice measurements from space. *Remote Sens. Environ.*, **99**, 187–219.
- Kayastha, R.B., Takeuchi, Y., Nakawo, M. and Ageta, Y. (2000): Practical prediction of ice melting beneath various thickness of debris cover on Khumbu Glacier, Nepal, using a positive degree-day factor. *In* Nakawo, M., Raymond, C.F. and Fountain, A. (eds.), *Debris-Covered Glaciers*, IAHS Publ., **264**, 71–81.
- Komori, J., Gurung, D.R., Iwata, S. and Yabuki, H. (2004): Variation and lake expansion of Chubda Glacier, Bhutan Himalayas, during the last 35 years. *Bull. Glaciol. Res.*, **21**, 49–55.
- Lundstrom, S.C., McCafferty, A.E. and Coe, J.A. (1993): Photogrammetric analysis of 1984–89 surface altitude change of the partially debris-covered Eliot Glacier, Mount Hood, Oregon, U.S.A. *Ann. Glaciol.*, **17**, 167–170.
- Mattson, L.E. and Gardner, J.S. (1991): Energy exchanges and ablation rates on the debris-covered Rakhiot Glacier, Pakistan. *Zeitschrift Für Gletscherkunde Und Glazialgeologie*, **25**, 17–32.
- Mattson, L.E., Gardner, J.S. and Young, G.J. (1993): Ablation on debris covered glaciers: an example from the Rakhiot Glacier, Punjab, Himalaya. *In* Young, G.J. (ed.), *Snow and Glacier Hydrology*, IAHS Publ., **218**, 289–296.
- McFeeters, S.K. (1996): The use of the Normalized Difference Water Index (NDWI) in the delineation of open water features. *Int. J. Remote Sens.*, **17**, 1425–1432.
- Naito, N., Nakawo, M., Kadota, T. and Raymond, C.F. (2000): Numerical simulation of recent shrinkage of Khumbu Glacier, Nepal Himalayas. *In* Nakawo, M., Raymond, C.F. and Fountain, A. (eds.), *Debris-Covered Glaciers*, IAHS Publ., **264**, 245–254.
- Nakawo, M. and Young, G.J. (1981): Field experiments to determine the effect of a debris layer on ablation of glacier ice. *Ann. Glaciol.*, **2**, 85–91.
- Nakawo, M. and Young, G.J. (1982): Estimate of glacier ablation under a debris layer from surface temperature and meteorological variables. *J. Glaciol.*, **28**, 29–34.
- Nakawo, M. and Rana, B. (1999): Estimate of ablation rate of glacier ice under a supraglacial debris layer. *Geografiska Annaler*, **81A**, 695–701.
- Nakawo, M., Iwata, S., Watanabe, O. and Yoshida, M. (1986): Processes which distribute supraglacial debris on the Khumbu Glacier, Nepal Himalayas. *Ann. Glaciol.*, **8**, 129–131.
- Nakawo, M., Moroboshi, T. and Uehara, S. (1993): Satellite data utilization for estimating ablation of debris covered glaciers. *In* Young, G.J. (ed.), *Snow and Glacier Hydrology*, IAHS Publ., **218**, 75–83.
- Ohata, T. and Higuchi, K. (1980): Heat balance study on glacier AX010 in Shorong Himal, East Nepal. *Seppyo*, **39**, Special issue, 42–47.
- Quincey, D.J., Lucas, R.M., Richardson, S.D., Glasser, N.F., Hambrey, M.J. and Reynolds, J.M. (2005): Optical remote sensing techniques in high-mountain environments: application to glacial hazards. *Prog. Phys. Geog.*, **29**, 475–505.
- Quincey, D.J., Richardson, S.D., Luckman, A., Lucas, R.M., Reynolds, J.M., Hambrey, M.J. and Glasser, N.F. (2006): Early recognition of glacial lake hazards in the Himalaya using remote sensing datasets. *Global Planet. Change*, in press. doi: 10.1016/j.gloplacha.2006.07.013.
- Rana, B., Nakawo, M., Fukushima, Y. and Ageta, Y. (1997): Application of a conceptual precipitation-runoff model (HYCMODEL) in a debris-covered glacierized basin in the Langtang Valley, Nepal Himalaya. *Ann. Glaciol.*, **25**, 226–231.
- Reynolds, J.M. (2000): On the formation of supraglacial lakes on debris-covered glaciers. *In* Nakawo, M., Raymond, C.F. and Fountain, A. (eds.), *Debris-Covered Glaciers*, IAHS Publ., **264**, 153–161.

- Richardson, S.D. and Reynolds, J.M. (2000): An overview of glacial hazards in the Himalayas. *Quatern. Int.*, **65/66**, 31–47.
- Sakai, A., Takeuchi, N., Fujita, K. and Nakawo, M. (2000): Role of supraglacial ponds in the ablation process of a debris-covered glacier in the Nepal Himalayas. *In* Nakawo, M., Raymond, C.F. and Fountain, A. (eds.), *Debris-Covered Glaciers*, IAHS Publ., **264**, 119–130.
- Suzuki, R., Fujita, K., Ageta, Y., Naito, N., Matsuda, Y. and Karma (2007): Meteorological observations during 2002–2004 in Lunana region, Bhutan Himalayas. *Bull. Glaciol. Res.*, **24**, 71–78.
- Takeuchi, Y., Kayastha, R.B. and Nakawo, M. (2000): Characteristics of ablation and heat balance in debris-free and debris-covered areas on Khumbu Glacier, Nepal Himalayas, in the pre-monsoon season. *In* Nakawo, M., Raymond, C.F. and Fountain, A. (eds.), *Debris-Covered Glaciers*, IAHS Publ., **264**, 53–61.
- Wessels, R.L., Kargel, J.S. and Kieffer, H.H. (2002): ASTER measurement of supraglacial lakes in the Mount Everest region of the Himalaya. *Ann. Glaciol.*, **34**, 399–408.
- Yamada, T. (1998): *Glacier Lake and its Outburst Flood in the Nepal Himalaya*. Monograph No. 1, Data Center for Glacier Research, Japanese Society of Snow and Ice, 96 pp.
- Yamada, T., Naito, N., Kohshima, S., Fushimi, H., Nakazawa, F., Segawa, T., Uetake, J., Suzuki, R., Sato, N., Karma, Chhetri, I.K., Gyenden, L., Yabuki, H. and Chikita, K. (2004): Outline of 2002 — research activities on glaciers and glacier lakes in Lunana region, Bhutan Himalayas. *Bull. Glaciol. Res.*, **21**, 79–90.